Supplement of Atmos. Chem. Phys., 15, 9109–9127, 2015
http://www.atmos-chem-phys.net/15/9109/2015/
doi:10.5194/acp-15-9109-2015-supplement

Atmospheric Chemistry and Physics Open Access

Supplement of

Aqueous-phase oligomerization of methyl vinyl ketone through photooxidation – Part 2: Development of the chemical mechanism and atmospheric implications

B. Ervens et al.

Correspondence to: B. Ervens (barbara.ervens@noaa.gov)

S1. Continuous-Flow EPR (electron paramagnetic resonance):

Transient radicals may be directly observed by mean of continuous-flow EPR. To use this technique for the present study, a steady state concentration of radicals was carried on the EPR cavity by pumping separated reactant solutions and mixing them prior the EPR cavity. The radicals were obtained using the following reactions:

$$Ti^{3+} + H_2O_2 \rightarrow Ti^{4+} + OH + OH^-$$

$$MVK + OH \rightarrow \text{Transient Radicals}$$

EPR experiments were carried out on a Bruker EMX instrument equipped with a TM4103 cylindrical cavity. Continuously degassed (Argon) aqueous solutions of MVK (25 mM (***Figure S1.1***) to 1 mM (***Figure S1.2***)) + H_2O_2 (25 to 10 mM, obtained from 30% H_2O_2 solution) and $Ti_2(SO_4)_3$ (2.5 mM (***Figure S1.1***) to 1 mM (***Figure S1.2***) obtained from a 20% aqueous solution in 1-4% sulfuric acid) were pumped by a 2 ways peristaltic pump (Cole-Parmer, typically 90 mL min^{-1}/stream) and injected into a flow cell fitted within the EPR cavity. A mixing chamber located prior the cell allowed for simultaneous mixing of the two streams (the concentrations indicated previously are those obtained after mixing).

Comparing our experimental EPR spectra to simulations (***Figure S1***), the signal of HO-CH_2-$^{\bullet}$CH-C(O)CH_3 radical adduct resulting from pathway (1) was clearly distinguished. The radical species which proportion was concentration dependent (compare ***Figures S1.1 and S1.2***) was attributed to a dimer radical such as HO-CH_2-CH(C(O)CH_3)-CH_2-$^{\bullet}$CH-C(O)CH_3, thus confirming the very fast oligomerization pathway (Gilbert et al., 1994). However, more than two radical species were present in our experiments, but their respective signals remained unidentified due to overlapping EPR lines in the spectra.

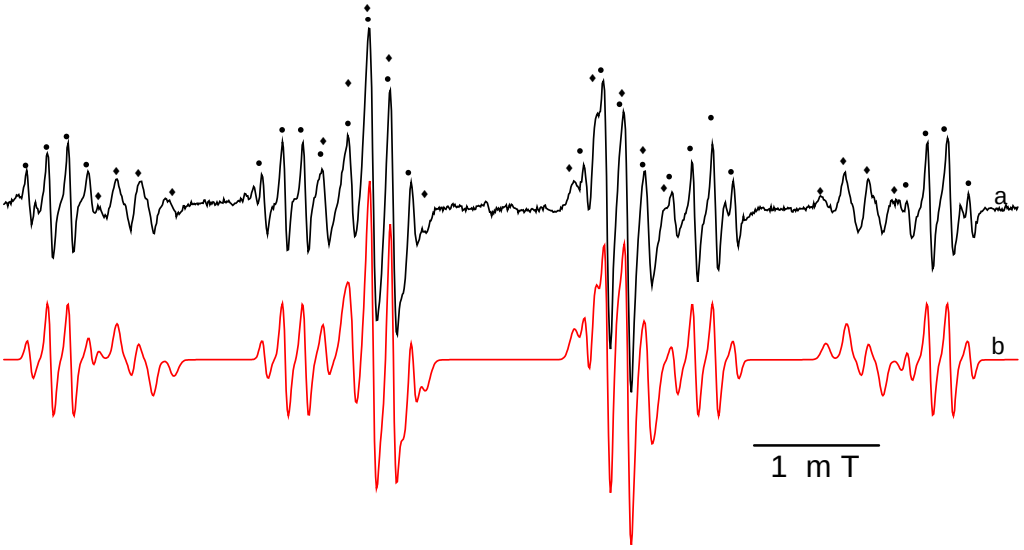

Figure S1.a: EPR spectra of radicals produced during reaction of hydroxyl radical with high initial concentrations of MVK (at pH = 1) : (**a**) experimental, (**b**) simulated. (•) HO-CH_2-˙CH-C(O)CH_3 transient radicals (♦)HO-CH_2-C(H)(C(O)CH_3)-CH_2-˙CH-C(O)CH_3 transient radicals. **[MVK] = 25 mM**, [Ti^{3+}] = 1.6 mM, [H_2O_2] = 16 mM, flow = 2x90 mL min^{-1}. Setting : Power : 20 mW, Gain : 10^6, Scan Width 8.2 mT, Modulation Amplitude : 0.05 mT, Time Constant 81.9 ms, Scan Time : 1342.1 s.

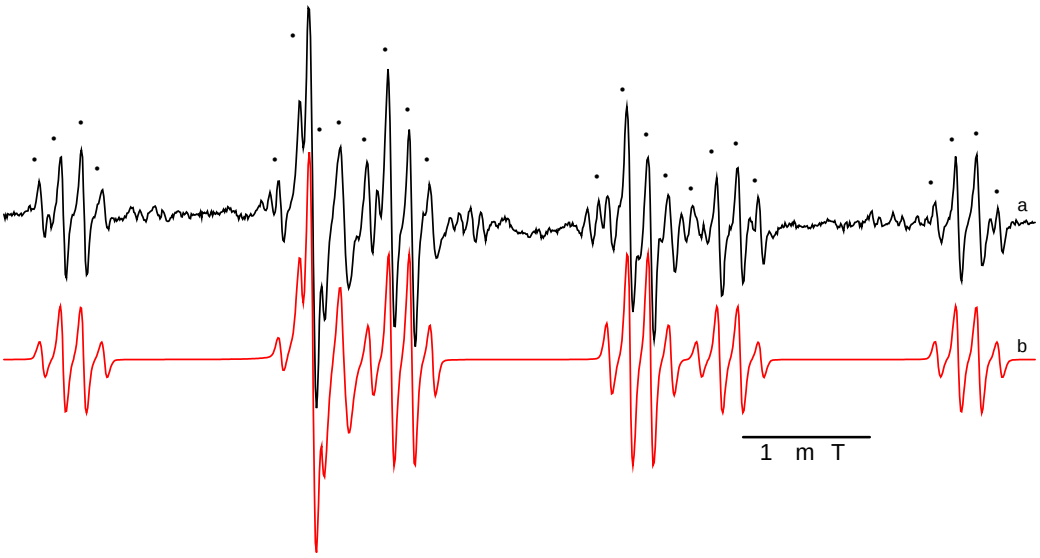

Figure S1b: EPR spectra of radicals produced during reaction of hydroxyl radical with low initial concentrations of MVK (at pH = 1): (**a**) experimental, (**b**) simulated. (•) HO-CH_2-˙CH-C(O)CH_3. **[MVK] = 1 mM**, [Ti^{3+}] = 1 mM, [H_2O_2] = 10 mM, flow = 2x90 mL min^{-1}. Setting : Power : 20 mW, Gain : 10^6, Scan Width 8.2 mT, Modulation Amplitude : 0.05 mT, Time Constant 81.9 ms, Scan Time : 1342.1 s.

S2. Fits to measured O_2 concentration during experiments

The solutions of MVK, H_2O_2 and O_2 were continuously stirred during the experiments. The concentration of dissolved oxygen was highly variable with time and cannot be reproduced by the box model as described in Section 2.2.1. The oxygen concentration was continuously measured during the experiments by an oxymeter (Consort C3020). In order to constrain the oxygen concentrations in the simulations of the experiments, the measured oxygen concentrations were empirically fitted. The corresponding equations and fits, together with the experimental data are included in Figure S2.

Supersaturation of dissolved O_2 was systematically observed prior MVK introduction, when H_2O_2 was photolyzed under our experimental conditions (Figure S2). This can be explained by the fact that our stirred reactor was closed prior MVK injection and samplings (to prevent from contamination by ambient air), and thus the aqueous/gas exchanges of O_2 were less efficient than for a fully open, stirred reactor. Thus, our solutions were sensitive to O_2 formation in the solution, which occurred through reactions 2, 3, 4, 5 and 6 in the H_2O_2 photolysis reaction scheme (Table S1). This also explains why the amount of O_2 produced increased with increasing initial H_2O_2 concentration (Figure S2), as the experiments were performed with different MVK and H_2O_2 concentrations, using a constant initial [MVK]/[H_2O_2] ratio. When MVK was introduced and during the rest of the experiment, the reactor was opened periodically for sampling, thus inducing aqueous/air exchanges of O_2, but these were less efficient than the reaction of O_2 consumption by the reaction as shown by the O_2 depletion observed.

HO_x reactions		
$H_2O_2 + h\nu \rightarrow 2\ OH$	$j_{H2O2} = f([MVK]_0)$	Estimated based on experiments, cf. Figure 3
$H_2O_2 + OH \rightarrow HO_2 + H_2O$	$3 \cdot 10^7\ M^{-1}\ s^{-1}$	(Christensen et al., 1982)
$HO_2 + HO_2/O_2^- \rightarrow O_2 + H_2O_2$	$8 \cdot 10^5\ M^{-1}\ s^{-1}$ (HO_2) $9.7 \cdot 10^7\ M^{-1}\ s^{-1}$ (O_2^-)	(Bielski et al., 1985)
$OH + HO_2/O_2^- \rightarrow H_2O + O_2$	$10^{10}\ M^{-1}\ s^{-1}$	(Elliot and Buxton, 1992)

Table S1: Reaction scheme for the photolysis of H_2O_2 and formation of O_2.

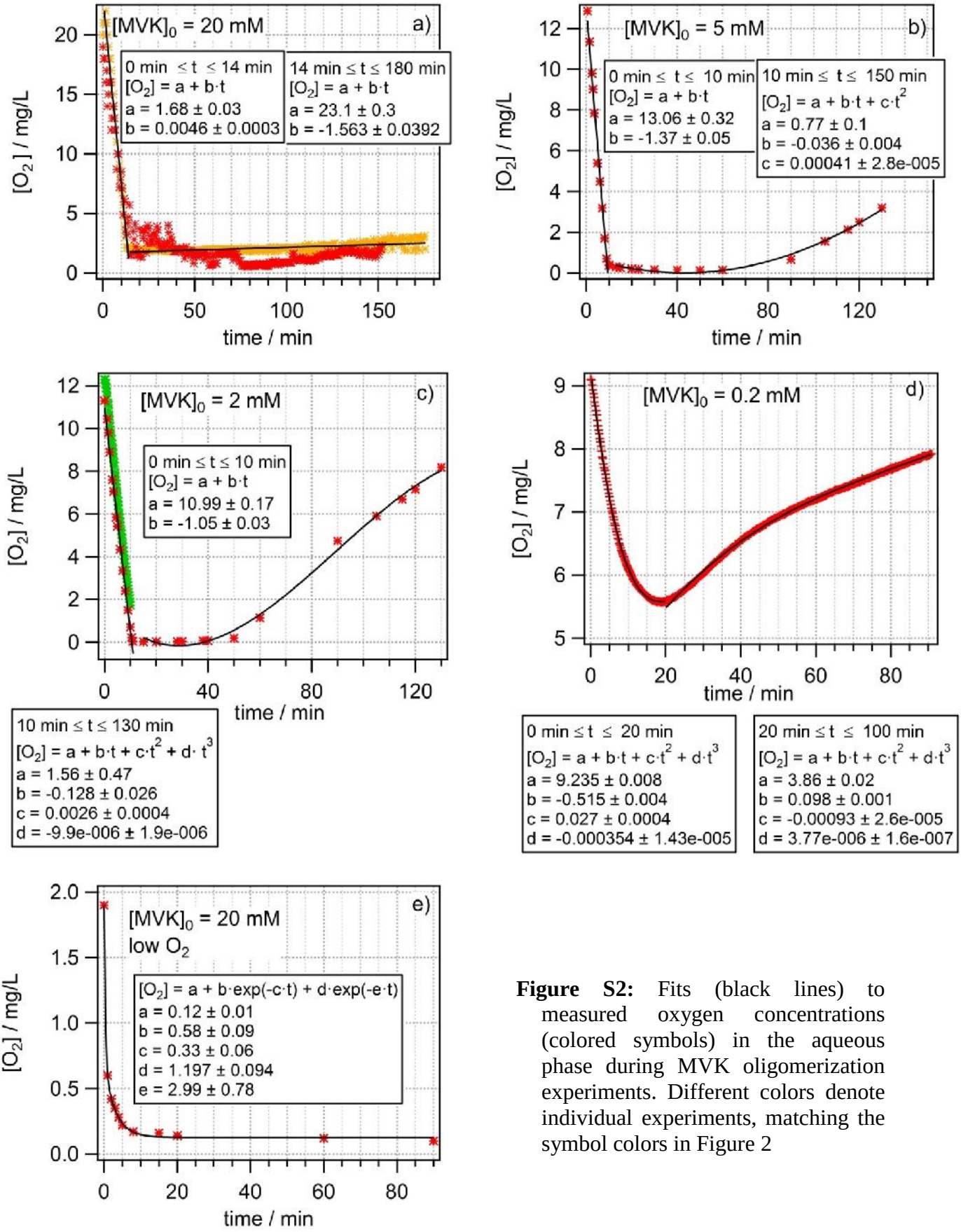

Figure S2: Fits (black lines) to measured oxygen concentrations (colored symbols) in the aqueous phase during MVK oligomerization experiments. Different colors denote individual experiments, matching the symbol colors in Figure 2

S3. Fits to measured pH values during experiments

The initial pH value for all experiments was pH = 6. Due to the formation of organic acids (e.g. acetic acids or possibly acid functionalities on the oligomers), the pH value decreased to pH = 3 ($[MVK]_0 \geq 2$ mM), and to pH = 4 for $[MVK]_0 = 0.2$ mM) over the course of the experiment. For simplicity, we constrain the pH value by linear fits for the time scales shown in ***Figure 2***.

$pH = a - b \cdot t$ $\quad a = 6$

$[MVK]_0 = 20$ mM $\quad b = 1/4800$

$[MVK]_0 = 2$ mM and 5 mM $\quad b = 1/2400$

$[MVK]_0 = 0.2$ mM $\quad b = 1/1500$

S4. Sensitivity studies of rate constants

Simulation	k_{arr} [s^{-1}]	k_{recomb} [s^{-1}]	k_{O2} [M^{-1} s^{-1}]	k_{olig} [M^{-1} s^{-1}]	k^{1st} [s^{-1}]	Comment
Base case	$8 \cdot 10^6$	$2.4 \cdot 10^6$	$3.1 \cdot 10^9$	$5 \cdot 10^7$	$6 \cdot 10^4$	
Multiplication factors						
#1	$\times 10^5$	$\times 10^5$				< 1% difference in MVK loss and oligomer mass as compared to Base Case; results not shown in Figure S3
#2	$/ 10^5$	$/ 10^5$				
#3			$\times 10$	$\times 10$		k_{O2} exceeds diffusion control limit; Base case k_{olig} is the upper limit of literature values
#4			/ 40	/ 8		
#5					/ 100	
#6				$\times 10$	$\times 100$	Base case k_{olig} is already at upper limit of literature values

Table S2: Sensitivity studies on estimated rate constants of the mechanism in Figure 1 and Table 1; results are shown in Figure S3.

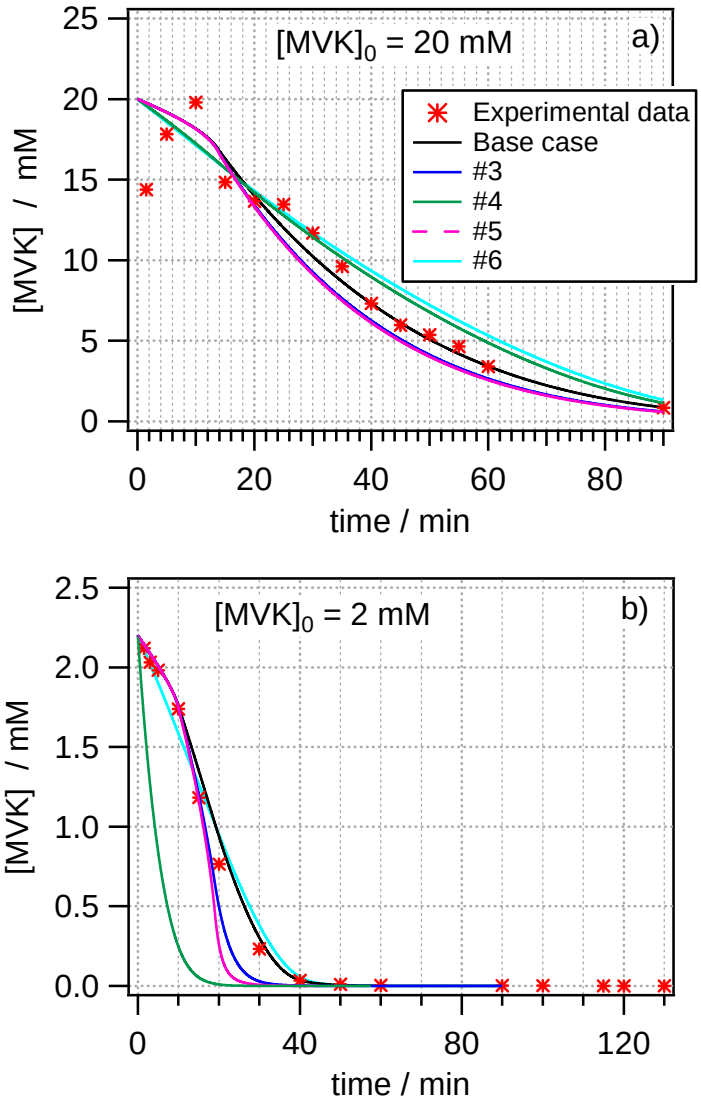

Figure S3: Results of sensitivity studies as listed in Table S2.
The black lines and the symbols are the same data as shown in Figure 2a and 2c, respectively.

Table S2 and Figure S3 summarize results of additional simulations using the mechanism in Figure 1. The most uncertain (estimated) rate constants were varied over several orders of magnitude. We did not include j_{H2O2}, k_{MVK}, and k_{loss} in these sensitivity studies since these constants are well constrained by our experiments (j_{H2O2}; Figure 3) or by literature studies (Doussin and Monod, 2013; Schöne et al., 2014).

The values of k_{arr} and k_{recomb} were varied together since they have been originally estimated based on the ratio k_{arr}/k_{recomb} for primary ethers. It seems unlikely that for similar compounds their ratio is different by several orders of magnitude. The fact that they do not impact the results in terms of MVK loss and oligomer formation shows that their values are not crucial for the results in Figure 2.

Variation of k_{O2} affects the competition between oligomer formation (all oligomer series,

except Oligomer 2; Figure 1). A higher k_{O2} leads to a less efficient MVK loss by oligomerization since fewer alkyl radicals are available to add further MVK molecules. In order to match the experimental data, k_{olig} has to be changed in the same direction to compensate the less efficient MVK loss. It should be noted that generally k_{O2} larger than ~10^{10} M^{-1} s^{-1} seem unlikely since this threshold is approximately the diffusion limit of chemical reactions in the aqueous phase. The review of peroxy radical formation reactions suggests that large, sterically-hindered molecules might have k_{O2} on the order of 10^8 M^{-1} s^{-1}. A lower rate constant of k_{olig} ($5 \cdot 10^7$ M^{-1} s^{-1} / 8 = $6.3 \cdot 10^6$ M^{-1} s^{-1} seems to match better literature values of similar reactions. However, such slow oligomerization cannot reproduce the fast MVK loss due to oligomerization as observed for the highest initial concentrations (Figure S3a) and overpredicts it at lower initial MVK concentrations (Figure S3b). The results are quite insensitive to the choice of the rate constant for the termination of the radical oligomerization, k^{1st} (Simulations #5 and #6) which supports our simplified approach of expressing this step as a first order process.

The comparison of Figures S3a and S3b shows that the chosen sets of rate constants ('Base case') are a robust representation of the mechanism in Figure 1 over a wide range of cocnentrations. Other combinations might lead to a good match for one of the concentrations whereas for others it fails to reproduce the observed data.

S5. One-step representation of oligomerization

Based on additional laboratory studies, it can be assumed that MACR also forms oligomers by a similar mechanism as shown in ***Figure 1***. Since a detailed mechanism as for MVK is not available, we describe the oligomer formation rate by a simplified scheme

$$\text{MVK or MACR} + \text{OH} \rightarrow \text{Oligomers} \qquad \text{(R-3)}$$

with k_{R-3}, chosen in a way that temporal evolution of the total oligomers in ***Figure 4*** for all cases is approximated. It is obvious that none of the rate constants fits exactly all cases: ***Figure S3*** shows the comparison of oligomer evolution as predicted by the full mechanism in ***Figure 1 and Table 1*** and the predicted oligomer masses as predicted replacing the full mechanism by R-S1. Best agreement is found for a values within the range of 10^9 M^{-1} s^{-1} < k_{R-3} < $1.5 \cdot 10^9$ M^{-1} s^{-1}, with a slightly higher value for the case using low initial oxygen concentrations ($k_{R-3} = 2 \cdot 10^9$ M^{-1} s^{-1}). Based on this analysis, the simulations in Section 4 are performed with $k_{R-3} = 1.5 \cdot 10^9$ M^{-1} s^{-1}.

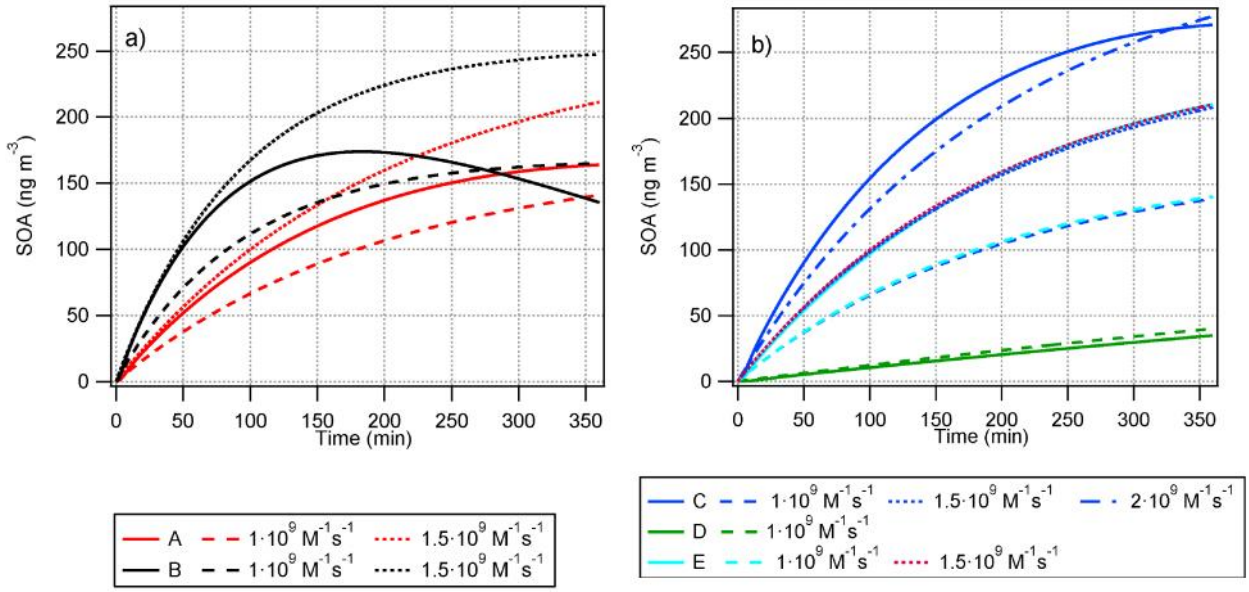

Figure S4: Predicted increase in oligomers in multiphase model (solid lines, these are the same results as in ***Figure 4***) and approximations for different $k_{R\text{-}S1}$ in order to represent oligomerization in a single step. Solid lines show results for the full mechanism; dashed lines are model results for several assumptions of $k_{R\text{-}3}$. Input data for Cases A-E are summarized in ***Table S3*** below. The best matching rate constant $k_{R\text{-}3}$ for each case is highlighted

Table S3: Assumptions of one-step rate constants $k_{R\text{-}3}$ to reproduce oligomer increase and decay for five sets of initial aqueous concentrations ($[MVK]_0$, $[O_2]_0$)

Case	**$[MVK]_0$ (mM)**	**$[O_2]_0$ («M)**	**$k_{R\text{-}3}$ (M^{-1} s^{-1})**
A	20	505	10^9 **$1.5\cdot10^9$**
B	5	436	**10^9** $1.5\cdot10^9$
C	20	60	10^9 $1.5\cdot10^9$ **$2\cdot10^9$**
D	0.2	284	$1.5\cdot10^9$
E	2	358	10^9 **$1.5\cdot10^9$**

References

Bielski, B. H. J., Cabell, D. E., Arudi, R. L., and Ross, A. B.: Reactivity of HO_2/O_2^- radicals in aqueous solution, J. Phys. Chem. Ref. Data, 14, 4,1041-1100, 1985.

Christensen, H., Sehested, K., and Corfitzen, H.: Reactions of hydroxyl radicals with hydrogen peroxide at ambient and elevated temperatures, J. Phys. Chem., 86, 9,1588-1590, 10.1021/j100206a023, 1982.

Doussin, J. F., and Monod, A.: Structure–activity relationship for the estimation of OH-oxidation rate constants of carbonyl compounds in the aqueous phase, Atmos. Chem. Phys., 13, 23,11625-11641, 10.5194/acp-13-11625-2013, 2013.

Elliot, A. J., and Buxton, G. V.: Temperature dependence of the reactions OH + O_2^- and OH + HO_2 in water up to 200^{o}C, J. Chem. Soc. Faraday Trans., 88,2465-2470, 1992.

Gilbert, B. C., Smith, J. R. L., Milne, E. C., Whitwood, A. C., and Taylor, P.: Kinetic and structural EPR studies of radical polymerization. Monomer, dimer, trimer and mid-chain radicals formed via the initiation of polymerization of acrylic acid and related compounds with electrophilic radicals ([radical dot]OH, SO4-[radical dot] and Cl2-[radical dot]), J. Chem. Soc., Perkin Transactions 2, 8,1759-1769, 10.1039/p29940001759, 1994.

Schöne, L., Schindelka, J., Szeremeta, E., Schaefer, T., Hoffmann, D., Rudzinski, K. J., Szmigielski, R., and Herrmann, H.: Atmospheric aqueous phase radical chemistry of the isoprene oxidation products methacrolein, methyl vinyl ketone, methacrylic acid and acrylic acid - kinetics and product studies, Phys. Chem. Chem. Phys., 16,6257-6272 10.1039/c3cp54859g, 2014.